Evaluation and comparison of Landsat 8, Sentinel-2 and Deimos-1 remote sensing indices for assessing burn severity in Mediterranean fire-prone ecosystems

Paula García-Llamas[a,b], Susana Suárez-Seoane[a,b], José Manuel Fernández-Guisuraga[a,b], Víctor Fernández-García[a,b], Alfonso Fernández-Manso[c], Carmen Quintano[d,e], Angela Taboada[a,b], Elena Marcos[a,b], Leonor Calvo[a,b]

P. García-Llamas (corresponding author)

e-mail: pgarcl@unileon.es; phone: 0034987291567

[a] Biodiversity and Environmental Management Dpt., Faculty of Biological and Environmental Sciences, University of León, Campus de Vegazana s/n, 24071, León, Spain

[b] Institute of Environmental Research (IMA), University of Léon, 24071, León, Spain

[c] Agrarian Science and Engineering Department, University of León, Av. Astorga s/n, 24400, Ponferrada, Spain

[d] Electronic Technology Department, University of Valladolid

[e] Sustainable Forest Management Research Institute, Universidad of Valladolid, Spanish National Institute for Agriculture and Food Research and Technology (INIA),

Date of the manuscript draft: February 2019

Manuscript word count: 6788

Abstract

The development of improved spatial and spectral resolution sensors provides new opportunities to assess burn severity more accurately. This study evaluates the ability of remote sensing indices derived from three remote sensing sensors (i.e., Landsat 8 OLI/TIRS, Sentinel-2 MSI and Deimos-1 SLIM-6-22) to assess burn severity (site, vegetation and soil burn severity). As a case study, we used a megafire (9,939 ha) that occurred in a Mediterranean ecosystem in northwestern Spain. Remote sensing indices included seven reflective, two thermal and four mixed indices, which were derived from each satellite and were validated with field burn severity metrics obtained from CBI index. Correlation patterns of field burn severity and remote sensing indices were relatively consistent across the different sensors. Additionally, regardless of the sensor, indices that incorporated SWIR bands (i.e., NBR-based indices), exceed those using red and NIR bands, and thermal and mixed indices. High resolution Sentinel-2 imagery only slightly improved the performance of indices based on NBR compared to Landsat 8. The dNDVI index from Landsat 8 and Sentinel-2 images showed relatively similar correlation values to NBR-based indices for site and soil burn severity, but showed limitations using Deimos-1. In general, mono-temporal and relativized indices better correlated with vegetation burn severity in heterogeneous systems than differenced indices. This study showed good potential for Landsat 8 OLI/TIRS and Sentinel-2 MSI for burn severity assessment in fire-prone heterogeneous ecosystems, although we highlight the need for further evaluation of Deimos-1 SLIM-6-22 in different fire scenarios, especially using bi-temporal indices.

Keywords: Composition Burn Index, remote sensing, thermal indices, spectral indices

1. Introduction

Burn severity, defined as the magnitude of the ecological change caused by fire (Lentile et al., 2006), has been identified as one of the most critical factors determining the ecological effect of fire on ecosystems (Tanase et al., 2011). It may affect post-fire plant regeneration dynamics, community composition and structure (Wang and Kemball 2003; Dzwonko et al., 2015), as well as increase degradation processes through the alteration of physical and chemical soil properties, microbial activity and soil erosion (Heydari et al., 2017). Consequently, the timely generation of reliable burn severity maps reflecting induced changes in vegetation and soil properties is of high priority for post-fire, short-term decision support (Miller et al., 2016).

Traditionally, burn severity evaluation has been conducted using field methods, such as the Composite Burn Index (CBI) and the GeoCBI index (Key and Benson 2006; De Santis and Chuvieco 2009). Nevertheless, field methods are usually costly and time-consuming, and provide limited spatial and temporal representation of post-fire ecological effects (Chuvieco et al., 2006). Fire causes substantial spectral and thermal changes on the land surface, associated with the consumption of vegetation and the exposure of soil and charred stems, which can be captured by remote sensing sensors (Epting et al., 2005; Mallinis et al., 2018). Based on these properties, remote sensing techniques provide a cost-effective alternative to field sampling to assess and quantify burn severity (Veraverbeke et al., 2011) over a wide range of temporal and spatial scales, and areas (Schepers et al., 2014).

Landsat multi-spectral sensors (30 m) provide one of the freely available, longest and most widely used collections of moderate spatial and spectral resolution imagery for monitoring burn severity (Eidenshink et al., 2007). Despite the widespread application of Landsat data, improved spatial, spectral and temporal resolution characteristics of

recently available satellite sensors is attracting increasing interest among fire researchers (Mallinis et al., 2018). In this context, satellite sensors like Sentinel-2 MSI and Deimos-1 SLIM-6-22 have desirable characteristics, including a higher spatial (i.e., 10-20 m and 22 m, respectively vs 30 m) and temporal (i.e., 5 days and 2-3 days respectively vs 16 days) resolution than Landsat data, which may provide better information for burn severity assessment. Recent studies by Fernández-Manso et al. (2016) and Navarro et al. (2017) successfully assessed burn severity based on Sentinel-2 data. Similarly, Gómez-Sánchez et al. (2017) showed a relatively good performance of Deimos-1 to evaluate burn severity. To our knowledge, this is the only study that has analyzed the potential of Deimos-1 imagery for monitoring post-fire effects. Moreover, the number of studies using Sentinel-2 for burn severity assessment remains limited. Therefore, despite earlier promising results, evaluation of such sensors is still a relevant area of research to refine and improve the generalization of remotely sensed measures of post-fire effects.

Most of the satellite-based burn severity studies use methods based on remote sensing indices due to their computational simplicity and straightforward application (Veraverbeke et al., 2012). Nevertheless, differences in the sensitivity of each spectral region to changes in soil and vegetation may result in different capabilities of remote sensing indices to discriminate fire effects (Chuvieco et al., 2006; Veraverbeke et al., 2011). Spectral indices based on the Near Infrared (NIR) and Short Wave Infrared (SWIR) bands, specifically the Normalized Burn Ratio (NBR) and its bi-temporal approaches, such as the differenced Normalized Burn Ratio (dNBR) and the Relativized differenced Normalized Burn Ratio (RdNBR), have been identified as optimal burn severity measures (Miller et al., 2009; Veraverbeke et al., 2010). Nevertheless, some authors (Roy et al., 2006; Escuin et al., 2008) have found those indices suboptimal in

describing burn severity. Other reflective indices like the Normalized Difference Vegetation Index (NDVI), the Soil Adjusted Vegetation Index (SAVI), the Enhanced Vegetation Index (EVI) and their bi-temporal counterparts have also shown good correlation with burn severity, even higher than NBR-based indices (Harris et al., 2011; Wu et al., 2015). Additionally, recent studies have begun to successfully incorporate thermal data for burn severity evaluation (Quintano et al., 2015, 2017) and for enhancing reflective indices' performance (Holden et al., 2005; Harris et al., 2011). Consequently, despite the numerous remote sensing indices developed in the literature to assess burn severity and the previous studies evaluating the potential of alternative sensors to Landsat for this purpose, there is no consensus about the optimal remote sensing indices and satellite sensor alternative (Mallinis et al., 2018). This fact highlights the need for further studies that evaluate the suitability of spectral indices and satellite sensors against field data for adequate burn severity assessment (Lentile et al., 2006).

The aim of this study was to evaluate the potential of Landsat 8 OLI/TIRS, Sentinel-2 MSI and Deimos-1 SLIM-6-22 imagery to quantitatively assess burn severity, using as a case study a megafire of 9,939 ha that occurred in a heterogeneous, forest-shrubland Mediterranean ecosystem in Spain. Specifically, we aimed: (i) to identify the most suitable sensor to assess site (vegetation plus soil), vegetation and soil burn severity; (ii) to detect the most capable remote sensing index from each sensor to discriminate site burn severity levels, as well as vegetation burn severity and soil burn severity individually, based on comparison with burn severity field measurements.

2. Material and methods

2.1. Study site

The study was conducted in the Cabrera mountain range (northwestern Spain; Figure 1) where 9,939 ha burned in August, 2017 (between 21th and 27th). This area is in the limit of the Mediterranean biogeographic region (Rivas-Martínez et al., 2011), with its climate classified as temperate, with maximum annual temperatures ranging from 8.7 to 29.4 ºC and a mean annual precipitation of 600-1500 mm. It has a rough and heterogeneous orography with altitudes ranging from 836 to 1,938 m.a.s.l. Soils are acidic, mainly originating from siliceous lithology such as slates. The area affected by the megafire was mainly covered by shrublands dominated by *Erica australis* and *Genista hystrix,* and forest dominated by *Quercus pyrenaica*. The fire occurred under relatively extreme weather conditions, with maximum temperatures of 35 ºC, low relative humidity values (35 %), and after a two-month drought episode. These extreme weather conditions increased the risk of fire and facilitated fire spread, resulting in large areas of high-severity effects.

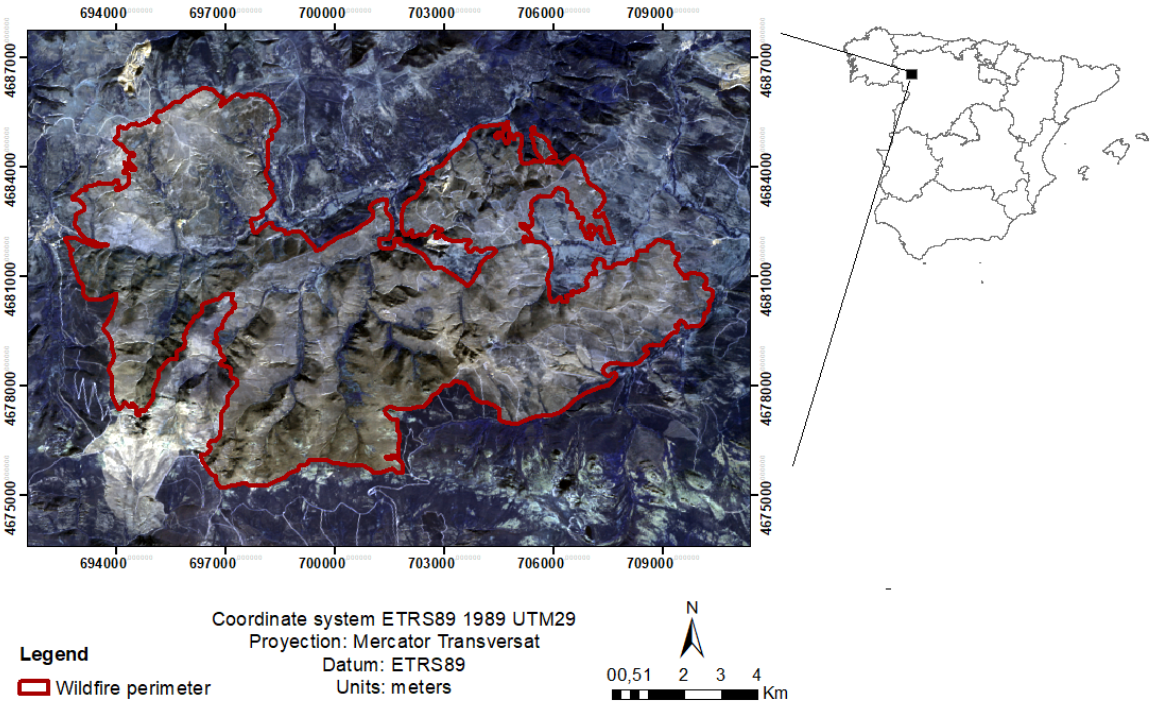

Figure 1. Location map of the study area (Sierra de la Cabrera, NW Spain) representing a false color composite post-fire image (10th October, 2017) obtained from Landsat 8 OLI/TIRS.

2.2. Field estimation of burn severity

Field data to measure burn severity were collected three months after the fire event. Fifty-three field plots of 30 m x 30 m size were distributed in fairly homogeneous patches across the study area, following a stratified random sampling design by type of vegetation (i.e., heathlands, gorse shrub lands and oak forests) to encompass all types of vegetation affected by fire. The sampling size was proportional to the extent covered by each type of vegetation, resulting in 20 plots in heathlands, 11 plots in gorse shrublands and 23 plots in oak forest. We further established 19 plots in unburned areas, which

were used as controls. Plot locations were georeferenced with a GPS receiver in post-processing mode (accuracy better than 0.50 m).

Assessment of site field burn severity was obtained following the protocol described by Fernández-García et al. (2018), which is an adaptation of the original CBI protocol developed by Key and Benson (2006). The procedure consisted on rating several variables from 0 (unburned) to 3 points (high severity) across five strata, to compute an average site burn severity using the average burn severity obtained per strata. Burn severity of vegetation and soil strata were also separately evaluated. See Fernández-García et al. (2018) for further details on the adapted CBI protocol.

2.3. *Remote sensing imagery and preprocessing*

Remote sensing information to estimate burn severity was obtained from three different data sources: the Landsat 8 OLI/TIRS, the Sentinel-2 MSI and the Deimos-1 SLIM-6-22 sensors. Landsat 8 OLI/TIRS imagery, at 30 m spatial resolution, includes nine reflective bands (i.e., three visible bands, two near-infrared [NIR] and short wave infrared bands [SWIR], one panchromatic band and two bands for describing aerosol, water vapor and cirrus clouds) and two thermal bands (United States Geological Survey 2015). Meanwhile, Sentinel-2 MSI has thirteen reflective bands (i.e., four 10 m visible and NIR bands; six 20 m red edge, NIR and SWIR bands; and three 60 m bands for characterizing aerosol, water vapor correction and cirrus clouds) (European Space Agency 2015). Deimos-1 SLIM-6-22 imagery is a 22 m spatial resolution product with three reflective bands (NIR, red, and green bands; https://earth.esa.int/documents/10174/2605161/DEIMOS-1-Imagery-User-Guide) (Figure 2).

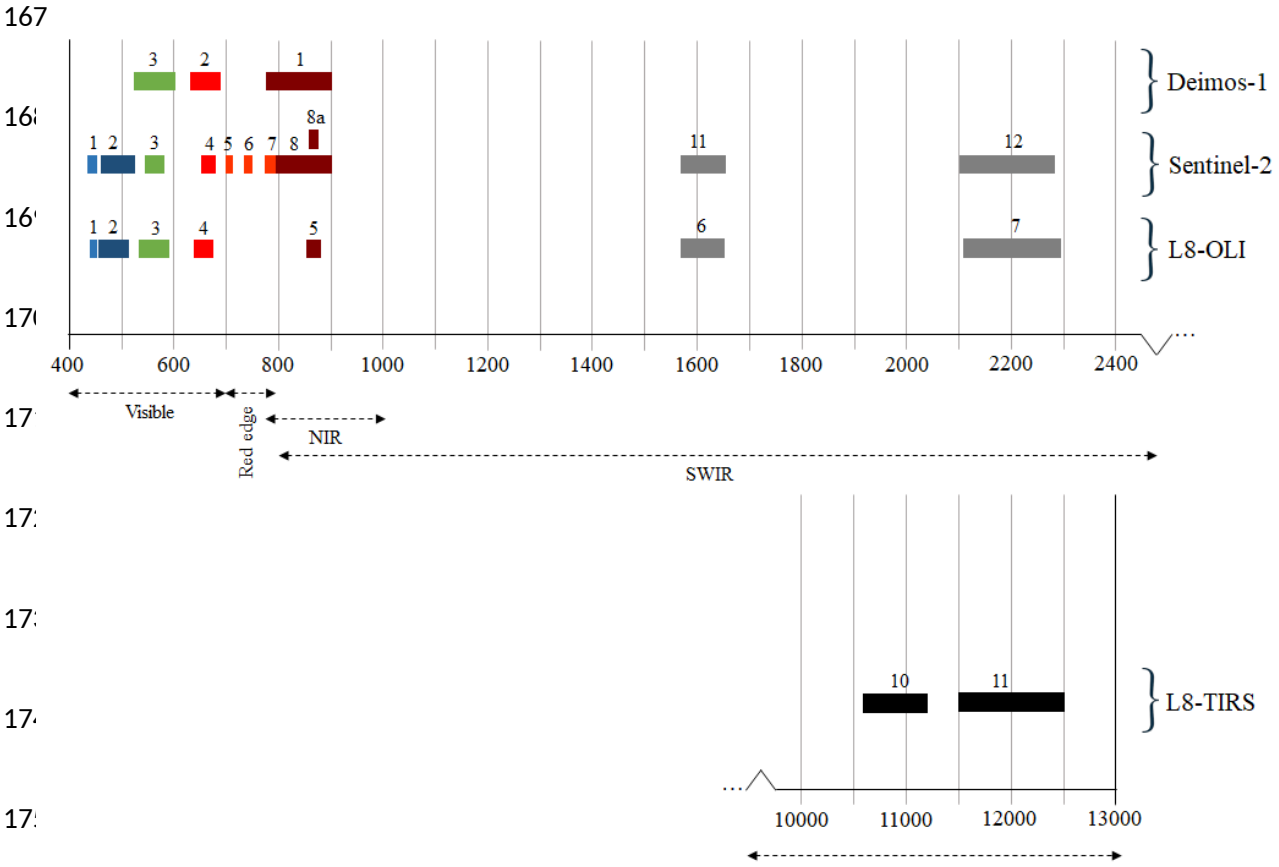

Figure 2. Comparison of spectral bands of Landsat 8 OLI/TIRS (L8-OLI and L8-TIRS), Sentinel-2 MSI and Deimos-1 SLIM-6-22 sensors.

Selected images to estimate burn severity included the available cloud-free pre- and post-fire images closest to the date of the fire, aiming to avoid phenological changes in the vegetation and to allow comparison among remote sensing products. Landsat 8 OLI/TIRS scenes were acquired on August 11th, 2017 (pre-fire image) and October 10th, 2017 (post-fire image) from the USG Earth Explorer server (United States Geological Survey, 1879); Sentinel 2 MSI scenes (C1-processing level) on August 13th, 2017 (pre-fire image) and September 2nd, 2017 (post-fire image) from the Copernicus server (European Space Agency 1975); and Deimos 1 SLIM-6-22 scenes on July 25th, 2017 (pre-fire image) and September 8th, 2017 (post-fire image).

188 The reflective bands of the three remote sensing products were atmospherically
189 corrected and converted to at-surface reflectance using the ATCOR atmospheric
190 correction model (Richter and Schläpfer 2018) included in the PCI GEOMATICS 2018
191 software. Furthermore, the thermal band (B10) of Landsat 8 was pre-processed and used
192 to obtain the Land Surface Temperature (LST) product following the method described
193 in Fernández-García et al. (2018).

194

195 **2.4. *Burn severity spectral indices***

196 Among the wide range of existing remote sensing metrics described in the literature, we
197 evaluated the performance of fourteen reflective, thermal and mixed (combining
198 reflective and thermal bands) spectral indices (Table 1). Specifically, selected indices
199 included: (i) seven reflective indices (NDVI, dNDVI, SAVI, NBR, dNBR, RdNBR,
200 EVI and dEVI – difference Enhanced Vegetation Index-); (ii) two thermal indices (LST
201 and dLST); and (iii) four mixed indices (NDVIT, SAVIT, (LST/EVI) and d(LST/EVI)).

202 NDVI, dNDVI and SAVI were calculated for Landsat 8 OLI/TIRS, Sentinel-2 MSI and
203 Deimos-1 SLIM-6-22. Concerning the Sentinel-2 MSI sensor, these indices were
204 created using the narrow NIR band (B8a) that has a high spectral correspondence with
205 the NIR band of Landsat 8 OLI (Figure 2). The SAVI index adds a soil calibration
206 constant (L) to the formula of NDVI to account for background effects (Schepers et al.,
207 2014). In our case, we considered a L value of 0.5, as this value has been recommended
208 for most environmental conditions (Epting et al., 2005).

209 The NBR, the dNBR and the RdNBR, as well as the EVI and the dEVI indices could
210 not be calculated with the Deimos-1 sensor because it does not capture data over blue
211 and SWIR regions (Figure 2). For the Sentinel-2 MSI sensor, these indices were derived

using the narrow NIR band (B8a) and the longer SWIR band (B12) to facilitate direct comparison among sensors (i.e., Landsat 8 OLI and Sentinel-2; Figure 2). Moreover, the spatial resolution of Sentinel-2 bands was homogenized by rescaling the SWIR band from 20 m to 10 m spatial resolution using the Nearest Neighbor rule. Thermal information was only available using the Landsat 8 OLI/TIRS sensor (Figure 2).

With the aim of enabling comparative analyses among satellites, values of spectral indices corresponding to each CBI plot were obtained by averaging the values extracted from raster pixels using 900 sampling points systematically distributed within each 30 m x 30 m CBI plot, according to the procedure described in Picotte and Robertson (2011).

Table 1. Spectral indexes evaluated and calculation algorithms, using Landsat 8 OLI/TIRS, Sentinel-2 MSI and Deimos-1 SLIM-6-22 spectral bands.

Spectral Index	Landsat 8 OLI/TIRS formula	Sentinel-2 MSI formula	Deimos-1 SLIM-6-22 formula	Reference
NDVI	$(\rho_5 - \rho_4)/(\rho_5 + \rho_4)$	$(\rho_{8A} - \rho_4)/(\rho_{8A} + \rho_4)$	$(\rho_1 - \rho_2)/(\rho_1 + \rho_2)$	Rouse et al. (1973)
dNDVI	$(NDVI_{pre} - NDVI_{post})$	$(NDVI_{pre} - NDVI_{post})$	$(NDVI_{pre} - NDVI_{post})$	Zhu et al. (2006)
SAVI	$(1 + L)[(\rho_5 - \rho_4)/(\rho_5 + \rho_4 + L)]$ with L = 0.5	$(1 + L)[(\rho_{8A} - \rho_4)/(\rho_{8A} + \rho_4 + L)]$ with L = 0.5	$(1 + L)[(\rho_1 - \rho_2)/(\rho_1 + \rho_2 + L)]$ with L = 0.5	Huete (1988)
NBR	$(\rho_5 - \rho_7)/(\rho_5 + \rho_7)$	$(\rho_{8A} - \rho_{12})/(\rho_{8A} + \rho_{12})$		López-García and Caselles (1991)
dNBR	$1000\ (NBR_{pre} - NBR_{post})$	$1000\ (NBR_{pre} - NBR_{post})$		Key (2006)
RdNBR	$(dNBR/(\lvert NBR_{pre}\rvert^{0.5})$	$(dNBR/(\lvert NBR_{pre}\rvert^{0.5})$		Miller and Thode (2007)
EVI	$2.5[(\rho_5 - \rho_4)/(\rho_5 + 6\rho_4 - 7.5\rho_2 + 1)]$	$2.5[(\rho_{8A} - \rho_4)/(\rho_{8A} + 6\rho_4 - 7.5\rho_2 + 1)]$		Gao et al. (2000)
dEVI	$(EVI_{pre} - EVI_{post})$	$(EVI_{pre} - EVI_{post})$		Zhu et al. (2006)
LST	LST in Kelvin from B_{10}	-		Yu et al. (2014)
dLST	$(LST_{pre} - LST_{post})$	-		Zheng et al. (2016)
NDVIT	$(\rho_5 - \rho_4 * \rho_{10})/(\rho_5 + \rho_4 * \rho_{10})$	-		Smith et al. (2007)
SAVIT	$(1 + L)[(\rho_5 - \rho_4 * \rho_{10})/(\rho_5 + \rho_4 * \rho_{10} + L)]$ with L = 0.5	-		Smith et al. (2007)
LST/EVI	$(LST - 273.15)/EVI$	-		Zheng et al. (2016)
d(LST/EVI)	$(LST/EVI)_{post} - (LST/EVI)_{post})$	-		Zheng et al. (2016)

2.5. *Statistical analyses*

Statistical correlations between field burn severity (i.e., site, vegetation and soil burn severity) and remote sensing indices derived from each satellite (Table 1) were estimated by fitting separated Ordinary Least Squares (OLS) models, following the approaches of previous studies (Epting et al., 2005; Quintano et al., 2015; Fernández-García et al., 2018). This procedure resulted in twenty-five models per site, vegetation and soil burn severity. Residuals of OLS models were graphically checked to ensure the appropriateness of models (i.e., assumptions of normal residuals' distribution, independence and homoscedasticity). The coefficient of determination (R^2) and the statistical significance of OLS models were used to compare the performance of the different spectral indexes, as well as the performance of the different remote sensing satellites. OLS model were run using the statistical software R (R Core Team, 2017).

3. Results

Comparing remote sensing satellites, Sentinel-2 MSI data, with the highest spatial resolution, slightly improved the performance of Landsat 8 OLI/TIRS to assess site, vegetation and soil burn severity, although only for indices including the SWIR and NIR bands. The availability of Landsat 8 thermal bands did not contribute to improving burn severity evaluation. Deimos-1 imagery only enabled the assessment of spectral indices based on the NIR and red bands. Additionally, it showed some limitations using bi-temporal indices (Table 2, 3 and 4).

Table 2. Coefficients of determination (R^2) and significance (p) of linear regression models between remote sensing indices derived from Landsat 8 OLI/TIRS, Sentinel-2 MSI and Deimos-1 SLIM-6-22 sensors and site burn severity estimated as CBI values. Maximum R^2 values for each satellite are in bold.

Remote sensing indices		Site burn severity		
		Landsat 8	Sentinel-2	Deimos-1
Reflective	NDVI	0.556***	0.467***	**0.481*** **
	dNDVI	**0.635*** **	**0.674*** **	0.420***
	SAVI	0.533***	0.520***	**0.517*** **
	NBR	**0.640*** **	**0.670*** **	
	dNBR	**0.690*** **	**0.767*** **	
	RdNBR	**0.686*** **	**0.762*** *	
	EVI	0.139**	0.005	
	dEVI	0.015	0.004	
Thermal	LST	0.119**		
	dLST	0.251***		
Mixed	NDVIT	0.406***		
	SAVIT	0.362***		
	dLST	0.251***		
	d(LST/EVI)	0.195***		

Significance of the correlations are represented as * $p < 0.05$; ** $p < 0.01$; *** $p < 0.001$

Table 3. Coefficients of determination (R^2) and significance (p) of linear regression models between remote sensing indices derived from Landsat 8 OLI/TIRS, Sentinel-2 and Deimos-1 sensors and vegetation burn severity estimated as CBI values. Maximum R^2 values for each satellite are in bold.

Remote sensing indices		Vegetation burn severity		
		Landsat 8	Sentinel-2	Deimos-1
Reflective	NDVI	0.631***	0.548***	**0.560*** **
	dNDVI	0.523**	0.569***	0.316**
	SAVI	0.589***	0.574***	**0.576*** **
	NBR	**0.696*** **	**0.721*** **	
	dNBR	0.578***	0.658***	
	RdNBR	**0.693*** **	**0.760*** **	
	EVI	0.072*	0.000	
	dEVI	0.000	0.000	
Thermal	LST	0.159***		
	dLST	0.187***		
Mixed	NDVIT	0.453***		
	SAVIT	0.426***		
	d(LST/EVI)	0.139**		
	LST/EVI	0.169***		

Significance of the correlations are represented as * $p < 0.05$; ** $p < 0.01$; *** $p < 0.001$

Table 4. Coefficients of determination (R^2) and significance (p) of linear regression models between remote sensing indices derived from Landsat 8 OLI/TIRS, Sentinel-2 and Deimos-1 sensors and soil burn severity estimated as CBI values. Maximum R^2 values for each satellite are in bold

Remote sensing indices		Soil burn severity		
		Landsat 8	Sentinel-2	Deimos-1
Reflective	NDVI	0.347**	0.25***	0.275**
	dNDVI	**0.607*** **	0.575***	**0.386*** **
	SAVI	0.328**	0.304***	0.320***
	NBR	0.416**	0.452***	
	dNBR	**0.623*** **	**0.686*** **	
	RdNBR	0.515***	0.596***	
	EVI	0.185***	0.002	
	dEVI	0.044**	0.026	
Thermal	LST	0.054*		
	dLST	0.275***		
Mixed	NDVIT	0.253***		
	SAVIT	0.213***		
	d(LST/EVI)	0.193***		
	LST/EVI	0.238***		

Significance of the correlations are represented as * $p < 0.05$; ** $p < 0.01$; *** $p < 0.001$

Focusing on remote sensing metrics, reflective indices based on NBR (i.e., NBR, dNBR and RdNBR) derived from Landsat 8 OLI and Sentinel-2 MSI best fitted field burn severity (Tables 2, 3). Nevertheless, they showed relatively lower correlation values for soil burn severity (Table 4).

The use of Sentinel-2 MSI data slightly improved results of NBR-based indices compared to Landsat 8 OLI (Table 2, 3 and 4; Figure 3). Specifically, dNBR and RdNBR correlated the best with site burn severity ($R^2 = 0.69$ and $R^2 = 0.76$ for Landsat 8 OLI and Sentinel-2 MSI respectively; Table 2), and more weakly with soil burn severity ($R^2 > 0.515$ and $R^2 = 0.596$ for Landsat 8 OLI/ and Sentinel-2 MSI respectively; Table 4). However, considering vegetation burn severity, NBR and RdNBR outperformed the dNBR index (Table 3).

The use of reflective indices based on NIR and red wavelength bands, such as the post-fire NDVI and SAVI, resulted in weaker relationships with field burn severity compared to NBR-based indices (Table 2, 3 and 4). Furthermore, correlation values of mono-temporal NDVI and SAVI indices did not significantly differ among remote sensing data sources. In detail, both NDVI and SAVI obtained a similar moderate correlation with site and vegetation burn severity ($R^2 > 0.47$ and $R^2 > 0.55$ for site and vegetation burn severity, respectively; Table 2 and 3), but were not able to match soil burn severity ($R^2 < 0.35$; Table 4). The bi-temporal dNDVI index considerably outperformed the post-fire NDVI index for site and soil burn severity and showed relatively similar correlation values to NBR-based indices, except when using Deimos-1 imagery (Table 2 and 4; Figure 3).

The reflective index EVI and its bi-temporal counterpart dEVI poorly correlated with site, vegetation and soil burn severity, and especially using Sentinel-2 MSI data ($R^2 \leq 0.18$ and $R^2 \geq 0.02$ for Landsat 8 OLI and Serntinel-2, respectively; Table 2, 3 and 4).

The inclusion of thermal information did not improve correlations with field burn severity compared to reflective indices. Both thermal and mixed indices derived from Landsat 8 OLI/TIRS did not work well in any case (i.e., with site, vegetation and burn severity), with the variance explained by models lower than 0.45 (Table 2, 3 and 4).

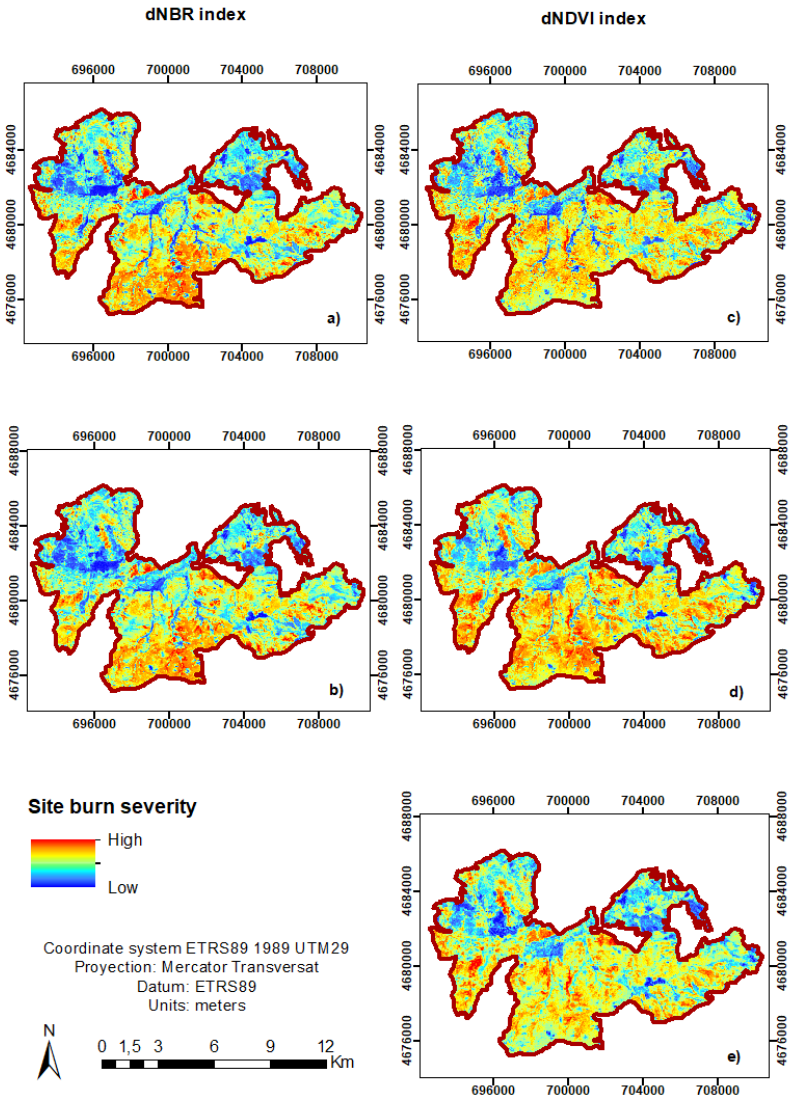

Figure 3. Site burn severity maps obtained using: a) dNBR index derived from Sentinel-2 MSI imagery; b) dNBR index derived from Landsat 8 OLI imagery; c) dNDVI index derived from Sentinel-2 MSI imagery; d) dNDVI index derived from Landsat 8 OLI imagery; e) dNDVI index derived from Deimos 1 SLIM-6-22.

4. Discussion

This study evaluates the suitability of individual Landsat 8 OLI/TIR, Sentinel-2 MSI and Deimos-1 SLIM-6-22 remote sensing indices in order to effectively assess fire severity in heterogeneous fire-prone Mediterranean ecosystems, dominated by shrublands and forest. Overall, correlation patterns of field burn severity (i.e., site, vegetation and soil burn severity) and remote sensing indices were consistent across different sensors. Furthermore, the results highlight that indices including NIR and SWIR bands better discriminated burn severity levels in heterogeneous landscapes, compared to indices based on NIR and red bands, and thermal and mixed metrics, as observed by Escuin et al. (2008) and Fernández-García et al. (2018).

Specifically, reflective indices based on NBR derived from both Landsat 8 OLI and Sentinel-2 MSI better correlated with field measurements of burn severity. The effectiveness of these indices to discriminate changes produced by fire is well established (Escuin et al., 2008; Veraverbeke et al., 2010, 2011), mainly due to the reduction of NIR reflectance, sensitive to chlorophyll content, and the increase in SWIR reflectance, related to a decrease in water content in vegetation and soil (Miller and Thode 2007). Indeed, in a study by Mallinis et al. (2018), comparing Landsat 8 and Sentinel-2, the most efficient in distinguishing fire effects was the NIR band of Landsat 8 and its corresponding wavelength band of Sentinel-2, the narrow NIR band (B8a), followed by the longer SWIR bands for both satellites. Similarly, Huang et al. (2016) also found that the narrow NIR band (B8a) and the longer SWIR band (B12) were the most suitable bands for detecting burned areas using a Sentinel-2 sensor.

Despite the overall good performance of NBR-based metrics, the response of individual indices differed among fire severities per strata. The dNBR and RdNBR strongly correlated with site burn severity, but more weakly with soil burn severity. Spectral

indices correlated better with surface variables than with soil, likely because of the shielding effect of vegetation on the ground and the inadequacies of passive sensors to see under vegetation canopy (Tanase et al., 2011). Thefore, our results corroborate certain limitations of remote sensing data to analyze fire effects on soil (Fernández-García et al., 2018). Considering vegetation burn severity, the NBR and RdNBR indices outperformed the dNBR index. This could be explained by the heterogeneity of pre-fire vegetation types (i.e. *Erica australis, Genista hystrix* and *Quercus pyrenaica*), with different chlorophyll content and canopy cover, which may bias burn severity estimates using dNBR due to the strong influence of pre-fire vegetation on the magnitude of this index (Safford et al., 2008; Wulder et al., 2009). Thus, the relativized RdNBR index, which provides information on the changes induced by fire regardless of pre-fire land cover (Miller and Thode 2007), may more accurately predict burn severity in heterogeneous landscapes (Safford et al., 2008; Miller et al., 2009). Further, mono-temporal NBR may help provide a more accurate burn severity assessment in heterogeneous systems, likely due to an attenuation of errors associated with differences in vegetation phenology and cover (Epting et al., 2005; Lhermitte et al., 2011). Abovementioned correlation patterns of individual NBR-based indices were similar for both Landsat 8 OLI and Sentinel-2 MSI data. Moreover, the use of higher-resolution Sentinel-2 MSI only slightly improved correlations with field-based burn severity, compared to their counterparts derived from Landsat 8 OLI. These results support the findings of Mallinis et al. (2018) and could be attributed to the high correspondence between the spectral response function of NIR and the narrow NIR bands (B8a) of Landsat 8 OLI and Sentinel-2 MSI, and between the SWIR bands of both sensors (Skakun et al., 2017; Figure 2).

426 Reflective indices based on NIR and red bands derived from Landsat OLI, Sentinel-2
427 MSI and Deimos-1, (i.e., the post-fire NDVI and SAVI indices), were similarly
428 correlated with field-based burn severity, but underperformed indices based on NBR.
429 Epting et al. (2005) and Veraverbeke et al. (2011) reported that indices including
430 information in the SWIR band (i.e., the NBR) were better suited than NDVI and SAVI
431 for distinguishing burn severity levels. Such underperformance was mainly observed for
432 soil burn severity. In this sense, the red band is strongly linked to vegetation chlorophyll
433 content that decreases in burned areas, but presents limited sensitivity to spectral post-
434 fire components of burned soil, such as black carbon or ash (Chuvieco et al., 2006;
435 Rocha and Shaver 2009). Conversely, the association of the SWIR band to moisture
436 content in vegetation and soil and charcoal variations would enhance sensitivity to
437 changes in soil properties after fire, such as the charcoal signal, scorching and dry soil
438 exposure, which would increase SWIR reflectance (Schepers et al., 2014).

439 The dNDVI index from Landsat 8 OLI and Sentinel-2 MSI data exceeded the NDVI
440 index for site and soil burn severity and showed relatively similar correlation
441 coefficients to NBR-based indices, contrary to studies by Chafer (2008) and
442 Veraverbeke et al. (2010). Consequently, the dNDVI index may substitute NBR-based
443 indices for assessing site and soil burn severity when imagery with a SWIR band is
444 unavailable. Nevertheless, similar to dNBR patterns, the dNDVI index showed a weaker
445 correlation with vegetation burn severity, probably due to the effect of the heterogeneity
446 of pre-fire vegetation types in terms of chlorophyll content and canopy cover (Todd and
447 Hoffer 1998; Lhermitte et al., 2011). Moreover, dNDVI from Deimos-1 data poorly
448 correlated with field burn severity. This heterogeneous pre-fire environment may
449 exhibit a complex spectrum signature difficult to discriminate with low spectral
450 resolution sensors (Rocchini 2007). Consequently, coarse spectral resolution in the NIR

and red bands of Deimos-1 could explain its reduced efficiency in evaluating burn severity based on the dNDVI index. To our knowledge, this is the second study that evaluates Deimos-1 imagery for burn severity assessment. Therefore, further research must be conducted under different fire scenarios aimed at determining the current potential of this sensor to detect burn severity, especially considering the unavailability of SWIR information.

The reflective post-EVI and dEVI indices seemed to be inefficient in assessing site, vegetation and soil burn severity, regardless of the sensor. There is still limited agreement on the functioning of those indices; while Schepers et al. (2014) noted a poor performance in ecosystems dominated by shrubs, Zheng et al. (2016) and Holden et al. (2010) found that correlations between the EVI and the dEVI and burn severity tended to increase in forest systems. These findings could suggest limitations of EVI and dEVI indices for assessing burn severity in shrubland ecosystems, likely because they are mostly tied to canopy structural characteristics, such as leaf area (Huete et al., 2002). Additionally, this poor performance may be associated with the inclusion of the blue band, which has less ability to discriminate burn areas, both with Landsat 8 OLI and Sentinel-2 MSI sensors (Mallinis et al., 2018).

Different studies support the utility of temperature data to assess burn severity (Veraverbeke et al., 2010; Quintano et al., 2017), likely because LST tends to increase after fire (Zheng et al., 2016). However, our study showed limitations of thermal data to determine field burn severity consistent with Harris et al. (2011) and Fernández-García et al. (2018). LST is strongly influenced by aspect and elevation (Vlassova et al., 2014; Quintano et al., 2015). Our study area is characterized by rough terrain and a wide altitudinal range that results in differences in insolation, moisture content, and vegetation type and cover, which ultimately affect LST (He et al., 2018). Therefore,

476 inconsistencies in our results compared to previous studies could be attributed to the
477 influence of topographic features on LST that lead to changes unassociated with burn
478 severity (Fernández-García et al., 2018).
479
480 **5. Conclusion**
481 This study represents a novel approach comparing the performance of several Landsat 8
482 OLI/TIRS, Sentinel-2 MSI and Deimos-1 remote sensing indices as suitable tools to
483 measure field burn severity in site, vegetation and soil in a very heterogeneous fire-
484 prone Mediterranean ecosystem dominated by shrublands and forest. It confirms that,
485 regardless of the sensor used, reflective NBR-based indices are more efficient in
486 evaluating burn severity than indices based on the red and NIR bands, and thermal
487 information. High resolution Sentinel-2 MSI imagery only slightly improved the
488 performance of NBR-based indices compared to Landsat 8 OLI. The dNDVI index
489 derived from Landsat 8 OLI and Sentinel-2 MSI correlated relatively well with site and
490 soil burn severity, demonstrating its potential for assessing burn severity when remote-
491 sensing imagery including SWIR information is unavailable. Moreover, mono-temporal
492 and relativized indices, exhibited a better correlation with vegetation burn severity in
493 heterogeneous systems compared to differenced indices. Results also highlighted the
494 limitations of remotely sensed indices in determining soil burn severity.
495 Products derived from Sentinel 2 and Landsat 8 showed a good potential for detecting
496 burn severity in a cost effective way, with minor differences between correlation
497 patterns of field burn severity and remote sensing indices. Nevertheless, we highlight
498 the need for further evaluation of the Deimos-1 sensor for different ecosystems,
499 especially when applying bi-temporal indices.
500

Acknowledgements

Funding for this study was provided by the Spanish Ministry of Economy and Competitiveness in the frame of projects GESFIRE (AGL2013-48189-C2-1-R) and FIRESEVES (AGL2017-86075-C2-1-R), and by the Regional Government of Castile and León in the frame of projects FIRECYL (LE033U14) and SEFIRECYL (LE001P17), and by the European Regional Development Fund. V. Fernández-García and J.M. Fernández-Guisuraga were supported by a predoctoral fellowship from the Ministry of Education, Culture and Sport of Spain (FPU14/00636 and FPU16/03070). We further thank Deimos Imaging for providing the images used in this study.

References

1. Chafer, C.J., 2008. A comparison of fire severity measures: an Australian example and implications for predicting major areas of soil erosion. Catena 74, 235-245. doi:10.1016/j.catena.2007.12.005

2. Chuvieco, E., Riaño, D., Danson, F.M., Martin, P., 2006. Use of a radiative transfer model to simulate the postfire spectral response to burn severity. Journal of Geophysical Research 11, G04S09. doi:10.1029/2005JG000143

3. Chuvieco, E., Kasischke, E.S., 2007. Remote sensing information for fire management and fire effects assessment. Journal of Geophysical Research 112, G01S90. doi:10.1029/2006JG000230

4. De Santis, A., Chuvieco, E., 2009. GeoCBI: a modified version of the Composite Burn Index for the initial assessment of the short-term burn severity from remotely sensed data. Remote Sensing of Environment 113(3), 554-562. doi.org/10.1016/j.rse.2008.10.011

5. Dzwonko, Z., Loster, S., Gawroński, S., 2015. Impact of fire severity on soil properties and the development of tree and shrub species in a Scots pine moist forest site in southern Poland. Forest Ecology and Management 342, 56-63. doi.org/10.1016/j.foreco.2015.01.013

6. Eidenshink, J., Schwind, B., Brewer, K., Zhu, Z.L., Quayle, B., Howard, S., 2007. A project for monitoring trends in burn severity. Fire ecology 3(1), 3-21.

7. Epting, J., Verbyla, D., Sorbel, B., 2005. Evaluation of remotely sensed indices for assessing burn severity in interior Alaska using Landsat TM and ETM+. Remote Sensing of Environment 96, 328-339. doi:10.1016/j.rse.2005.03.002

8. Escuin, S., Navarro, R., Fernández, P., 2008. Fire severity assessment by using NBR (Normalized Burn Ratio) and NDVI (Normalized Difference Vegetation Index)

derived from LANDSAT TM/ETM images. International Journal of Remote Sensing 29(4), 1053-1073. doi.org/10.1080/01431160701281072

9. European Space Agency, 2015. Copernicus open access hub. https://scihub.copernicus.eu/dhus/#/home (accessed 11 October 2018)

10. European Space Agency, 2015. User guides SENTINEL-2 MSI introduction. https://sentinel.esa.int/web/sentinel/user-guides/sentinel-2-msi (accessed 20 October 2018)

11. Fernández-García, V., Santamarta, M., Fernández-Manso, A., Quintano, C., Marcos, E., Calvo, E., 2018. Burn severity metrics in fire-prone pine ecosystems along a climatic gradient using Landsat imagery. Remote Sensing of Environment 206, 205-217. doi.org/10.1016/j.rse.2017.12.029

12. Fernández-Manso, A., Fernández-Manso, O., Quintano, C., 2016. SENTINEL-2A red-edge spectral indices suitability for discriminating burn severity. International Journal of Applied Earth Observation and Geoinformation 50, 170-175. doi.org/10.1016/j.jag.2016.03.005

13. Gao, X., Huete, A.R., Ni, W., Miura, T., 2000. Optical-biophysical relationships of vegetation spectra without background contamination. Remote Sensing of Environment 74(3), 609-620. doi.org/10.1016/S0034-4257(00)00150-4

14. Gómez-Sánchez, E., de las Heras, J., Lucas-Borja, M., Moya, D., 2017. Ajuste de metodologías para evaluar severidad de quemado en zonas semiáridas (SE peninsular): incendio Donceles 2012. Revista de Teledetección 49, 103-113. doi.org/10.4995/raet.2017.7121

15. Harris, S., Veraverbeke, S., Hook, S., 2011. Evaluating spectral indices for assessing fire severity in chaparral ecosystems (southern California) using

MODIS/ASTER (MASTER) airbone simulator data. Remote Sensing 3, 2403-2419. doi:10.3390/rs3112403

16. He, J., Zhao, W., Li, A., Wen, F., Yu, D., 2018. The impact of the terrain effect on land surface temperature variation based on Landsat-8 observations in mountainous areas. International Journal of Remote Sensing 1-20. doi: 10.1080/01431161.2018.1466082

17. Heydari, M., Rostamy, A., Najafi, F., Dey, D.C., 2017. Effect of fire severity on physical and biochemical soil properties in Zagros oak (*Quercus brantii* Lindl.) forests in Iran. Journal of Forestry Research 28(1), 95-104. doi 10.1007/s11676-016-0299-x

18. Holden, Z.A., Smith, A.M.S., Morgan, P., Rollins, M.G., Gessler, P.E., 2005. Evaluation of novel thermally enhanced spectral indices for mapping fire perimeters and comparisons with fire atlas data. International Journal of Remote Sensing 26(21), 4801-4808. doi:10.1080/01431160500239008

19. Holden, Z.A., Morgan, P., Smith, A.M., Vierling, L., 2010. Beyond Landsat: a comparison of four satellite sensors for detecting burn severity in ponderosa pine forests of the Gila Wilderness, NM, USA. International Journal of Wildland Fire 19, 449-458.

20. Huang, H., Roy, D.P., Boschetti, L., Zhang, H.K., Yan, L., Kumar, S.S., Gomez-Dans, J., Li, J., 2016. Separability analysis of Sentinel-2A Multi-Spectral Instrument (MSI) data for burned area discrimination. Remote Sensing 8(10), 873. doi:10.3390/rs8100873

21. Huete, A.R., 1988. A Soil-Adjusted Vegetation Index (SAVI). Remote Sensing of Environment 25, 295-309.

22. Huete, A., Didan, K., Miura, T., Rodriguez, E.P., Gao, X., Ferreira, L.G., 2002. Overview of the radiometric and biophysical performance of the MODIS vegetation

indices. Remote Sensing of Environment 83, 195-213. doi.org/10.1016/S0034-4257(02)00096-2

23. Key, C.H., 2006. Ecological and sampling constraints on defining landscape fire severity. Fire Ecology 2(2), 34-59. doi.org/10.4996/fireecology.0202034

24. Key, C.H., Benson, N.C., 2006. Landscape Assessment (LA) sampling and analysis methods. USDA Forest Service General Technical Reports RMRS-GTR-164-CD.

25. Lentile, L.B., Holden, Z.A., Smith, A.M.S., Falkowski, M.J., Hudak, A.T., Morgan, P., Lewis, S.A., Gessler, P.E., Benson, N.C., 2006. Remote sensing techniques to assess active fire characteristics and post-fire effects. International Journal of Wildland Fire 15, 319-345. doi.org/10.1071/WF05097

26. Lhermitte, S., Verbesselt, J., Verstraeten, W.W., Veraverbeke, S., Coppin, P., 2011. Assessing intra-annual vegetation regrowth after fire using the pixel based regeneration index. ISPRS Journal of Photogrammetry and Remote Sensing 66, 17-27. doi:10.1016/j.isprsjprs.2010.08.004

27. López-García, M.J., Caselles, V., 1991. Mapping burns and natural reforestation using thematic mapper data. Geocarto International 6(1), 31-37. doi.org/10.1080/10106049109354290

28. Mallinis, G., Mitsopoulos, I., Chrysafi, I., 2018. Evaluating and comparing Sentinel 2A and Landsat-8 Operational Land Imager (OLI) spectral indices for estimating fire severity in a Mediterranean pine ecosystem of Greece. GIScience & Remote Sensing 55(1), 1-18. doi:10.1080/15481603.2017.1354803

29. Miller, J.D., Thode, A.E., 2007. Quantifying burn severity in a heterogeneous landscape with a relative version of the Delta Normalized Burn Ratio (dNBR). Remote Sensing of Environment 109, 66-80. doi.org/10.1016/j.rse.2006.12.006

30. Miller, J.D., Knapp, E.E., Key, C.H., Skinner, C.N., Isbell, C.J., Creasy, R.M., Sherlock, J.W., 2009. Calibration and validation of the relative differenced Normalized Burn Ratio (RdNBR) to three measures of fire severity in the Sierra Nevada and Klamath Mountains, California, USA. Remote Sensing of Environment 113(3), 645-656. doi:10.1016/j.rse.2008.11.009

31. Miller, M.E., Elliot, W.J., Billmire, M., Robichaud, P.R., Endsley, K.A., 2016. Rapid-response tools and datasets for post-fire remediation: linking remote sensing and process-based hydrological models. International Journal of Wildland Fire 25(10), 1061-1073. doi.org/10.1071/WF15162

32. Navarro, G., Caballero, I., Silva, G., Parra, P.C., Vázquez, Á., Caldeira, R., 2017. Evaluation of forest fire on Madeira Island using Sentinel-2A MSI imagery. International Journal of Applied Earth Observation and Geoinformation 58, 97-106. doi.org/10.1016/j.jag.2017.02.003

33. Picotte, J.J., Robertson, K.M., 2011. Validation of remote sensing of burn severity in south-eastern US ecosystems. International Journal of Wildland Fire 20(3), 453-464. doi.org/10.1071/WF10013

34. Quintano, C., Fernández-Manso, A., Calvo, L., Marcos, E., Valbuena, L., 2015. Land surface temperature as potential indicator of burn severity in forest Mediterranean ecosystems. International Journal of Applied Earth Observation and Geoinformation 36, 1-12. doi.org/10.1016/j.jag.2014.10.015

35. Quintano, C., Fernández-Manso, A., Roberts, D.A., 2017. Burn severity mapping from Landsat MESMA fraction images and Land Surface Temperature. Remote sensing of environment 190, 83-95. doi.org/10.1016/j.rse.2016.12.009

36. Vv R Core Team 2017. R: a language and environment for statistical computing. Available from: https://www.R-project.org/

37. Richter, R., Schläpfer, D., 2018. "Atmospheric / Topographic Correction for Satellite Imagery". DLR report DLR-IB 565-01/2018, Wessling, Germany, pp 280.

38. Rivas-Martínez, S., Rivas-Sáenz, S., Penas A., 2011. Worldwide bioclimatic classification system. Global Geobotany 1, 1-634 + 4 Maps.

39. Rocha, A.V., Shaver, G.R., 2009. Advantages of a two band EVI calculated from solar and photosynthetically active radiation fluxes. Agricultural and Forest Meteorology 149, 1560-1563. doi:10.1016/j.agrformet.2009.03.016

40. Rocchini, D., 2007. Effects of spatial and spectral resolution in estimating ecosystem α-diversity by satellite imagery. Remote Sensing of Environment 111(4), 423-434. doi.org/10.1016/j.rse.2007.03.018

41. Roy, D.P., Boschetti, L., Trigg, S.N., 2006. Remote sensing of fire severity: assessing the performance of the normalized burn ratio. IEEE Geoscience and Remote Sensing Letters 3(1), 112-116. doi: 10.1109/LGRS.2005.858485

42. Rouse, J.W., Haas, R.H., Schell, J.A., Deering, D.W., 1973. Monitoring vegetation systems in the great plains with ERTS. In: Proceedings of the Third ERTS Symposium. NASA SP-351, 1. NASA, Washington DC, U.S., pp. 309-317.

43. Safford, H.D., Miller, J., Schmidt, D., Roath, B., Parsons, A., 2008. BAER soil burn severity maps do not measure fire effects to vegetation: a comment on Odion and Hanson (2006). Ecosystems 11, 1-11. doi: 10.1007/s10021-007-9094-z

44. Schepers, L., Haest, B., Veraverbeke, S., Spanhove, T., Vanden Borre, J., Goossens, R., 2014. Burned area detection and burn severity assessment of a heathland fire in Belgium using airborne imaging spectroscopy (APEX). Remote Sensing 6(3), 1803-1826. doi:10.1016/j.agrformet.2009.03.016

45. Smith, A.M.S., Drake, N.A., Wooster, M.J., Hudak, A., Holden, Z.A., Gibbons, C.J., 2007. Production of Landsat ETM+ reference imagery of burn areas within southern African savannahs: comparison of methods and application to MODIS. International Journal of Remote Sensing 28(12), 2753-2775. doi.org/10.1080/01431160600954704

46. Skakun, S., Vermote, E., Roger, J.C., Franch, B., 2017. Combined use of Landsat-8 and Sentinel-2A images for winter crop mapping and winter wheat yield assessment at regional scale. Geosciences 3(2), 163-186. doi:10.3934/geosci.2017.2.163

47. Tanase, M., de la Riva, J., Pérez-Cabello, F., 2011. Estimating burn severity at the regional level using optically based indices. Canadian Journal of Forest Research 41(4), 863-872. doi:10.1139/X11-011

48. Todd, S.W., Hoffer, R.M., 1998. Responses of spectral indices to variations in vegetation cover and soil background. Photogrammetric Engineering & Remote Sensing 64(9), 915-921

49. United States Geological Survey, 2015. Landsat 8 (L8) data users handbook version 1.5 https://landsat.usgs.gov/sites/default/files/documents/LSDS-1574_L8_Data_Users_Handbook.pdf (accessed 15 October 2018)

50. United States Geological Survey, 2015. United States Geological Survey server. https://earthexplorer.usgs.gov/ (accessed 10 October 2018)

51. Veraverbeke, S., Verstraeten, W.W., Lhermitte, S., Goossens, R., 2010. Evaluating Landsat Thematic Mapper spectral indices for estimating burn severity of the 2007 Peloponnese wildfires in Greece. International Journal of Wildland Fire 19(5), 558-569. doi.org/10.1071/WF09069

52. Veraverbeke, S., Lhermitte, S., Verstraeten, W.W., Goossens, R., 2011. Evaluation of pre/post-fire differenced spectral indices for assessing burn severity in a Mediterranean environment with Landsat Thematic Mapper. International Journal of Remote Sensing 32(12), 3521-3537. doi.org/10.1080/01431161003752430

53. Veraverbeke, S., Hook, S., Hulley, G., 2012. An alternative spectral index for rapid fire severity assessments. Remote Sensing of Environment 123, 72-80. doi:10.1016/j.rse.2012.02.025

54. Vlassova, L., Pérez-Cabello, F., Rodrigues Mimbrero, M., Montorio Llovería, R., García-Martín, A., 2014. Analysis of the relationship between land surface temperature and wildfire severity in a series of Landsat images. Remote Sensing 6, 6136-6162. doi:10.3390/rs6076136

55. Wang, G.G., Kemball, K.J., 2003. The effect of fire severity on early development of understory vegetation following a stand replacing wildfire. In: 5th Symposium on Fire and Forest Meteorology jointly with 2nd International Wildland Fire Ecology and Fire Management Congress, Orlando, FL, pp. 16-20.

56. Wu, Z., Middleton, B., Hetzler, R., Vogel, J., Dye, D., 2015. Vegetation burn severity mapping using Landsat-8 and WorldView-2. Photogrammetric Engineering & Remote Sensing 81(2), 143-154. doi: 10.14358/PERS.81.2.143

57. Wulder, M.A., White, J.C., Alvarez, F., Han, T., Rogan, J., Hawkes, B., 2009. Characterizing boreal forest wildfire with multi-temporal Landsat and LIDAR data. Remote Sensing of Environment 113, 1540-1555. doi:10.1016/j.rse.2009.03.004

58. Zheng, Z., Zeng, Y., Li, S., Huang, W., 2016. A new burn severity index based on land surface temperature and enhanced vegetation index. International Journal of Earth Observation and Geoinformation 45, 84-94. doi.org/10.1016/j.jag.2015.11.002

59. Zhu, Z., Key, C., Ohlen, D., Benson, N., 2006. Evaluate sensitivities of burn-severity mapping algorithms for different ecosystems and fire histories in the United States. In: Final Report to the Joint Fire Science Program, Project JFSP 01-1-4-12, p. 35.

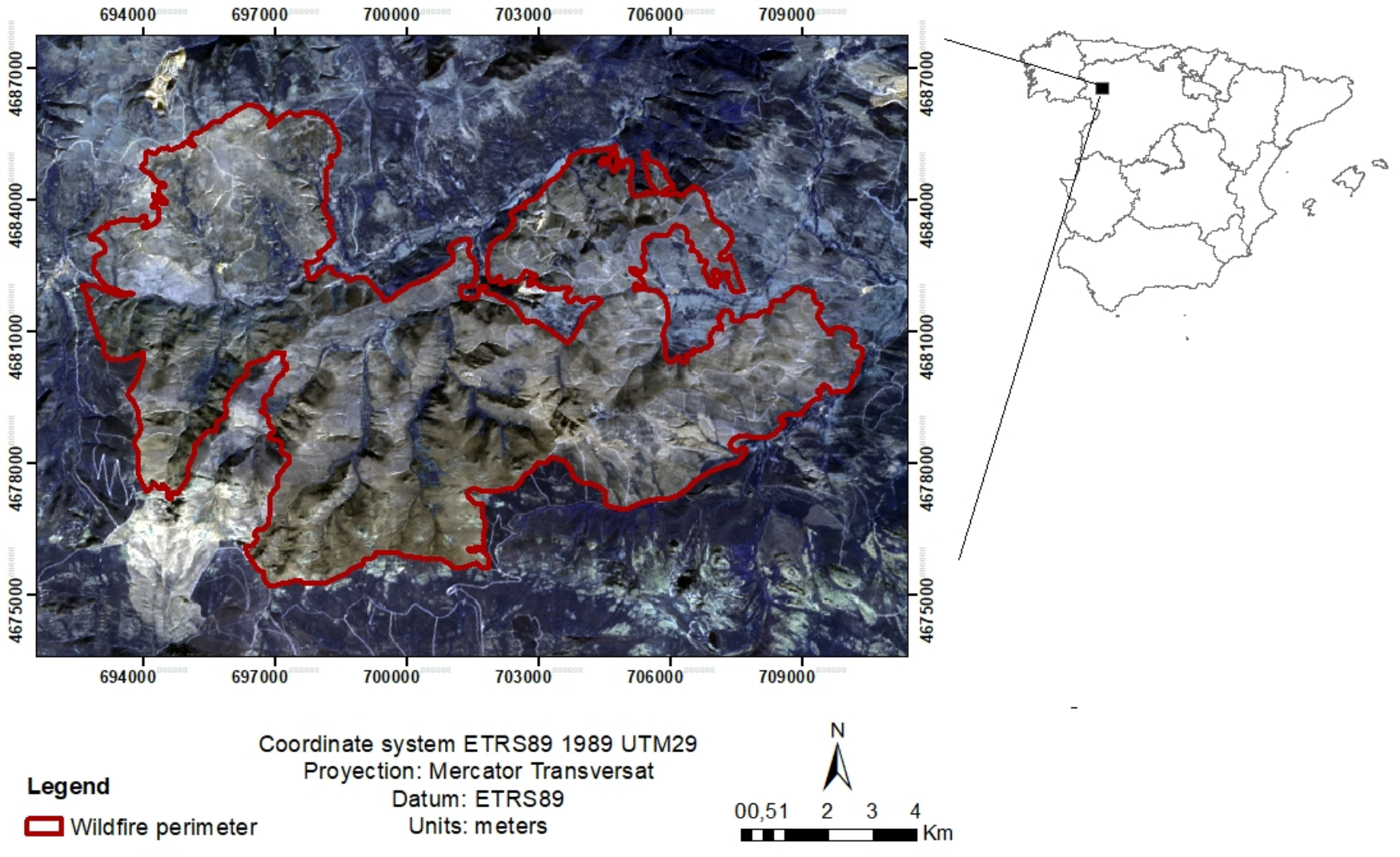
694000
697000
700000
703000
706000
709000
4687000
4684000
4681000
4678000
4675000
Coordinate system ETRS89 1989 UTM29
Proyection: Mercator Transversat
Datum: ETRS89
Units: meters
Legend
Wildfire perimeter
N
00,51 2 3 4
Km

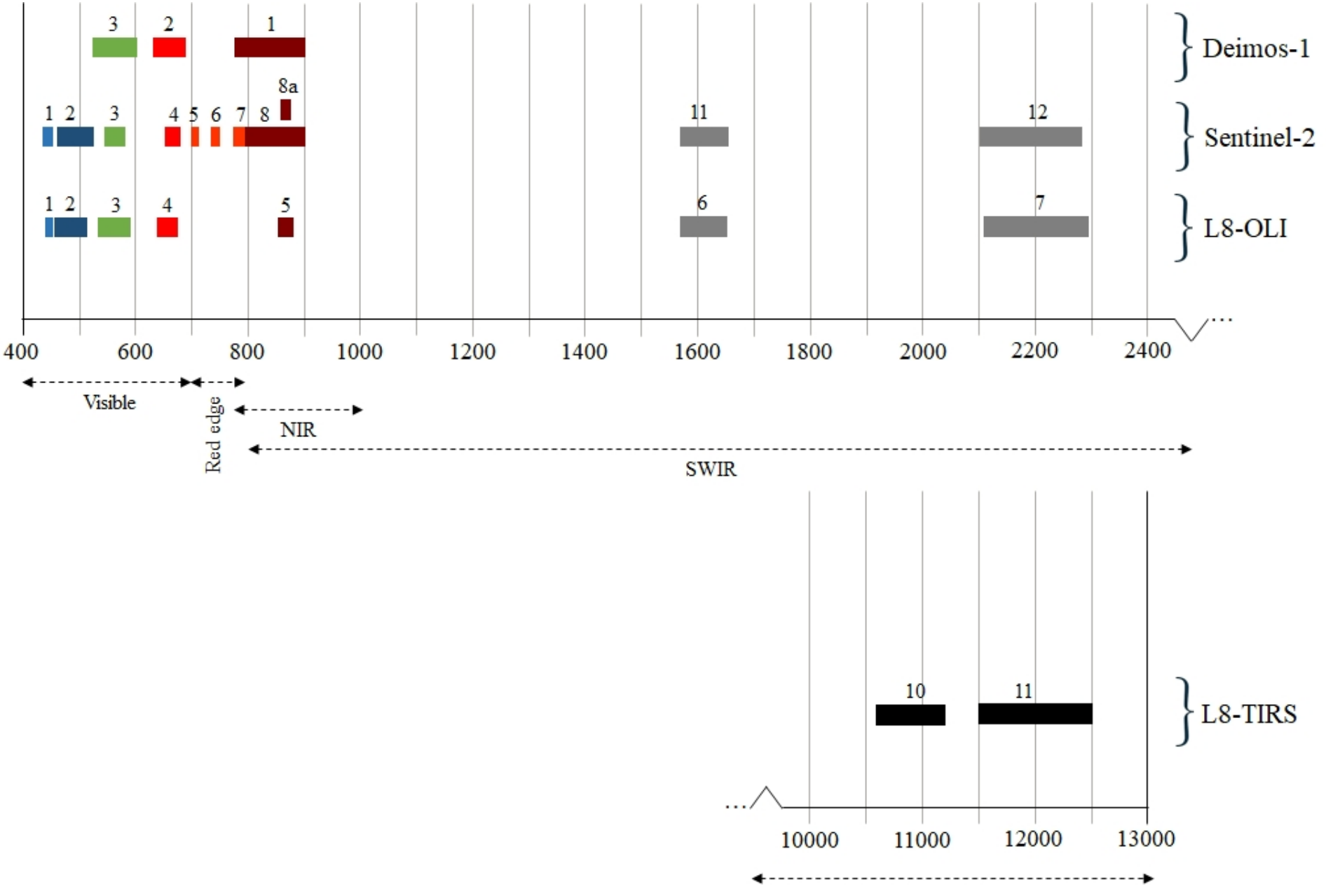
3
2
1
8a
1 2
3
4 5 6 7 8
11
12
1 2
3
4
5
6
7
Deimos-1
Sentinel-2
L8-OLI
400
600
800
1000
1200
1400
1600
1800
2000
2200
2400
Visible
Red edge
NIR
SWIR
10
11
L8-TIRS
10000
11000
12000
13000

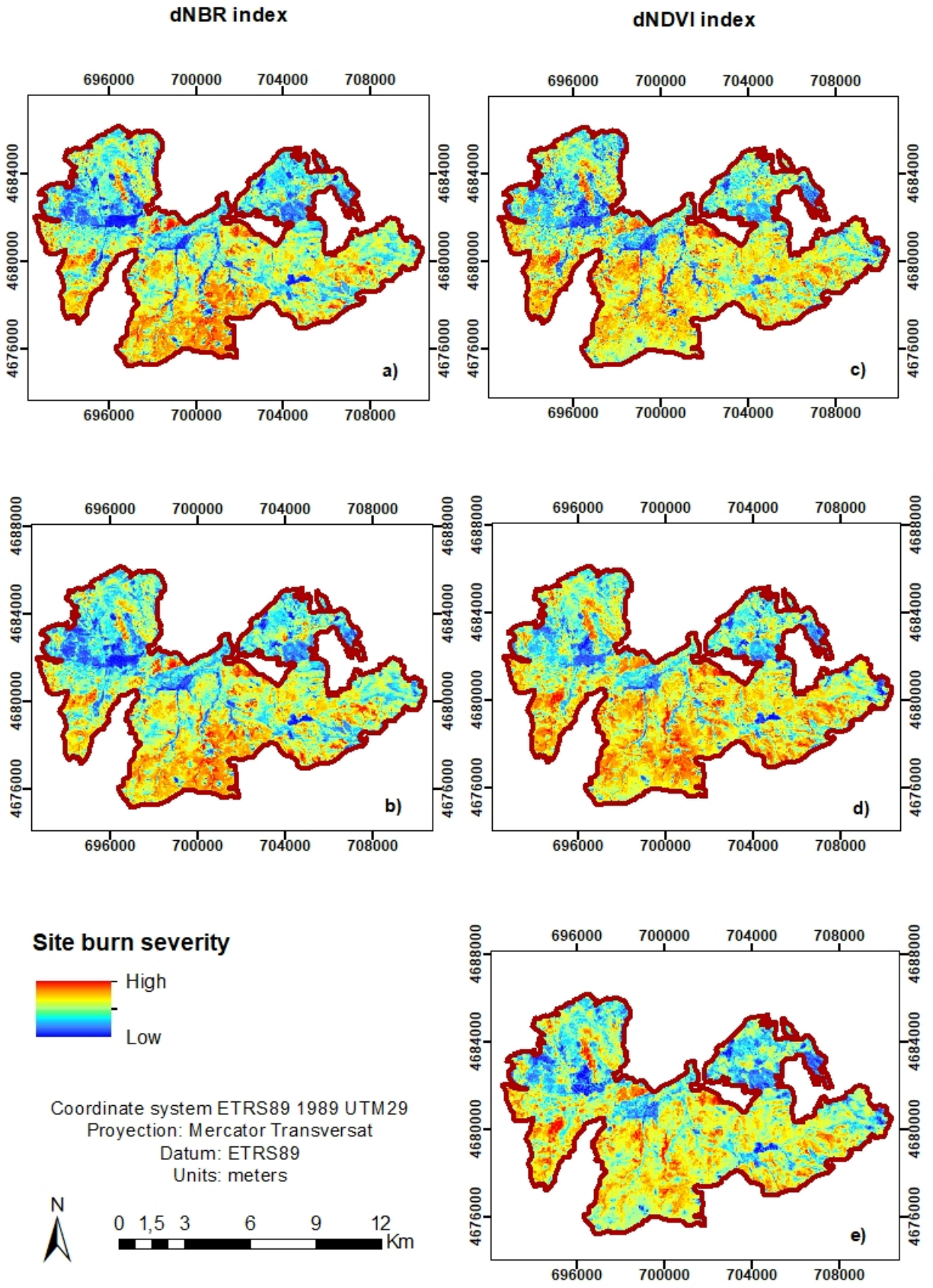
dNBR index
dNDVI index
696000
700000
704000
708000
4676000
4680000
4684000
4688000
a)
b)
c)
d)
e)
Site burn severity
High
Low
Coordinate system ETRS89 1989 UTM29
Proyection: Mercator Transversat
Datum: ETRS89
Units: meters
N
0 1,5 3 6 9 12
Km

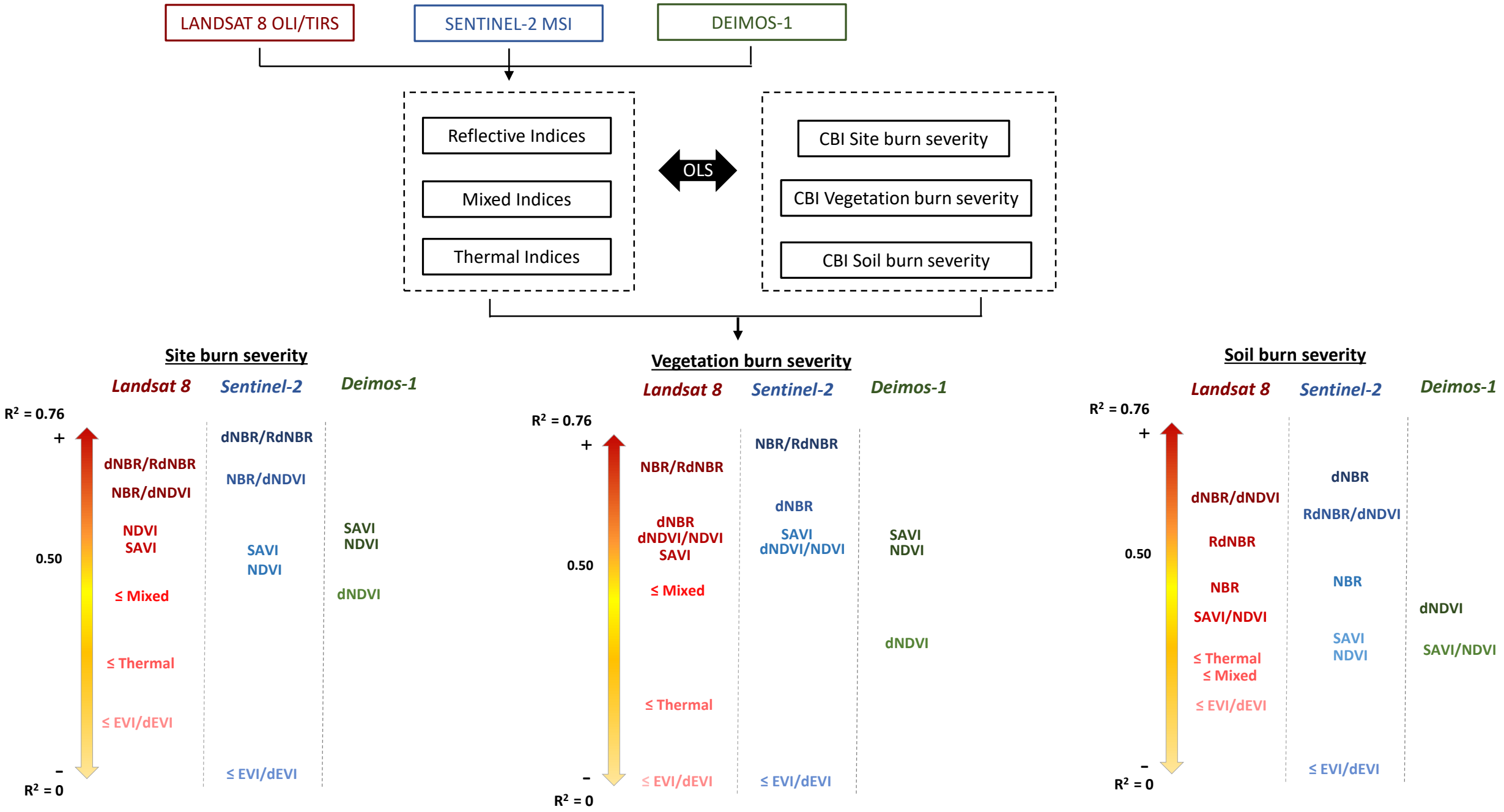

Figure1. Coefficients of determination (R^2) of OLS models between remote sensing índices from Landsat 8 OLI/TIRS, Sentinel-2 and Deimos-1; and site, vegetation and soil burn severity